NANO LETTERS

Letter

pubs.acs.org/NanoLett

Gap Plasmons and Near-Field Enhancement in Closely Packed Sub-10 nm Gap Resonators

Thomas Siegfried,*[,†] Yasin Ekinci,[†] Olivier J. F. Martin,[‡] and Hans Sigg[†]

[†]Laboratory for Micro- and Nanotechnology, Paul Scherrer Institut, 5232 Villigen-PSI, Switzerland

[‡]Nanophotonics and Metrology Laboratory, EPFL, 1015 Lausanne, Switzerland

Supporting Information

ABSTRACT: Pairs of metal nanoparticles with a sub-10 nm gap are an efficient way to achieve extreme near-field enhancement for sensing applications. We demonstrate an attractive alternative based on Fabry–Perot type nanogap resonators, where the resonance is defined by the gap width and vertical elongation instead of the particle geometry. We discuss the crucial design parameters for such gap plasmons to produce maximum near-field enhancement for surface-enhanced Raman scattering and show compatibility of the pattern processing with low-cost and low-resolution lithography. We find a minimum critical metal thickness of 80 nm and observe that the mode coupling from the far field increases by tapering the gap opening. We also show the saturation of the Raman signal for nanogap periodicities below 1 μm, demonstrating efficient funneling of light into such nanogap arrays.

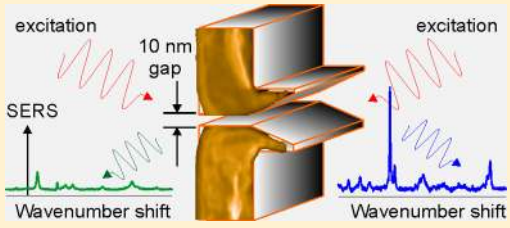

KEYWORDS: *Nanogap, gap plasmon, surface-enhanced Raman scattering, near-field enhancement, light funneling, Fabry–Perot*

The generation of electromagnetic hot spots with extreme near-field enhancement is the prerequisite for plasmonic sensing applications, especially for detection down to the single molecule level.[1−6] Few nanometer separations between noble metal nanoparticles are known to produce such extreme near-field enhancements and are thus often used to design nanostructures for practical applications.[6−14] Commonly, the near-field is enhanced with decreasing gap size, with an ultimate limit of roughly 0.5 nm before charge recombination occurs through electron tunneling.[15,16]

However, an effective sensing platform should not only aim at strong near-field localization but also provide efficient coupling to the incident field, good reproducibility of the nanostructures, and a high density of the hot spots. For nanoantenna patterns, such as arrays of closely spaced bowtie antenna, the coupling efficiency is primarily defined by the individual antenna plasmon resonance which can be slightly shifted by the coupling to the neighboring structures.[15] Nanoantenna have been studied extensively and can be fabricated cost-effectively,[17,18] but control over few-nanometer gap separations was so far only realized by electron beam lithography (EBL),[9,10,15] electromigration,[14] spacing layers,[8] or shadow evaporation.[12,13] Such nanometer-precise lithographic processes are extremely challenging and cost-intensive, while offering only low throughput and are limited to a small sensing area with only a few nanogaps (i.e., a low filling factor). A notable exception is nanosphere lithography offering wafer-size arrays of nanoparticles by direct assembly or angular evaporation;[17,19] the tuning of the particle shape, metal layer thickness, and gap size is however limited.

Recently, strong near-field enhancement from nanometer slit arrays was demonstrated over large areas using scalable processes such as atomic layer deposition[11,20] (ALD) or glancing angular deposition[21] (GLAD). Such slits support gap plasmons which are created by lateral electromagnetic coupling between two opposing metallic surfaces. The upper and lower boundary of the slit can lead to Fabry–Perot interferences similar to a metal–insulator–metal (MIM) waveguide.[22−24]

Here, we present a comprehensive study of the geometry required to obtain nanogap resonators which exhibit strong near-field enhancement. In particular, we study the role of the gap size and gap elongation on the gap plasmon mode. We show that surface-enhanced Raman scattering (SERS) critically depends on the resonance matching of the incident field with the gap plasmon mode. Furthermore, increased coupling efficiency by funneling of the incident light through a tapered geometry is demonstrated. We finally show saturation of the SERS signal for nanogap densities higher than 1 μm^{-1}.

The periodic nanogap arrays in our study were fabricated in a simple one-step process combining EUV interference lithography[25,26] and angular evaporation.[27] Precise control of gap sizes even below 10 nm was obtained for both 1D and 2D periodic arrays of different thicknesses, without the need of further fabrication steps such as lift-off and etching which would jeopardize sub-10 nm accuracy.[21] The Au is evaporated at grazing angles onto a grating pattern of transparent HSQ photoresist, such that by shadowing the opposite grating sidewall an elongated vertical channel with nanometric width is obtained (schematic and details in Figure S1 of the Supporting Information).[21] The gap size is primarily defined by the resist

Received: August 13, 2013
Revised: October 2, 2013
Published: October 10, 2013

   dx.doi.org/10.1021/nl403030g | *Nano Lett.* 2013, 13, 5449−5453

mask dimensions, the angle of incidence, and the deposition thickness. For a given metal thickness, the gap size is varied by changing the duty cycle of the resist pattern with the exposure and development time. The resulting gap size can be predicted with a geometric model combined with an analytic factor and is additionally determined by the analysis of several top and cross sectional scanning electron microscope (SEM) images. Evaporating multiple substrates simultaneously, we find similar gap sizes deviating by only few nanometers and also that the measured SERS signal intensity does not vary by more than 15%. Although we use high-resolution lithography in this work, it should be emphasized that our approach only depends on the abrupt vertical sidewalls which can also be well-produced by low-cost nanosphere, nanoimprint, or laser interference lithography.[17,28] A 1-nm-thick Cr layer evaporated under normal incidence forms an effective adhesion layer which does not affect the plasmonic performance of the system.[29] The cross-section and top-view SEM images of the obtained sub-10 nm gap arrays are shown in Figure 1a and b.

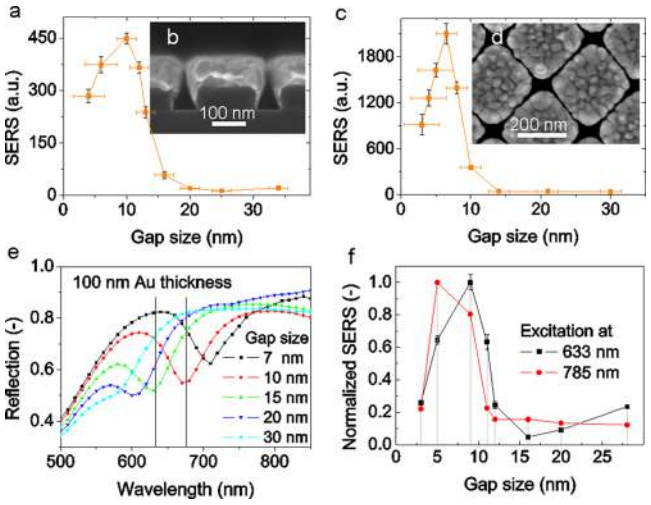

Figure 1. Gap plasmon modes and SERS intensity for varying nanogap sizes. Experimental SERS intensities for (a) 1D gratings with a period of 250 nm and (c) 2D nanodot arrays with a period of 280 nm. SEM micrographs of (b) the cross section of a 1D grating and (d) the top view of the 2D nanodot array with a Au thickness of the 95 nm and a gap size of roughly 10 nm. (e) Calculated gap plasmon modes for a 1D grating with varying gap sizes. The Raman excitation and detection wavelength are marked in the spectrum. (f) SERS intensity at excitation wavelengths of 633 and 785 nm for a 1D grating with varying gap sizes. The intensities correspond to the 1008 cm^{-1} peak of a self-assembled benzene-ethane-thiol monolayer. Error bars represent the standard deviation of 16 spatially separated SERS measurements and the analysis of multiple SEM images.

For nanogap sizes below 30 nm, the measured SERS intensity increases strongly for both 1D and 2D nanogap arrays, shown in Figure 1c and d, respectively. The SERS intensity for the 1D case is polarization-dependent with maximal intensity for the electric field aligned perpendicular (TM) to the gap.[21] We find larger SERS signals from the 2D gap resonators, which could be attributed to better coupling efficiency of the 2D pattern mediated by the large hole in the crossing of two gaps (Figure 1d), compared to a 1D grating. Additionally, the 2D pattern is insensitive to the polarization, and the angular evaporation process is simplified by a continuous substrate rotation, while the 1D pattern requires frequent substrate tilting. Gap plasmon modes are calculated with a full-field numerical method based on a surface integral formulation of Maxwell's equations.[30] Computed reflectance for nanogap resonators with varying gap sizes is shown in Figure 1e. The resonant plasmonic modes appear in reflection as a dip and are found to red-shift from 570 to 710 nm when the gap size is reduced from 30 to 7 nm. The SERS enhancement is found to peak at gap sizes for which the nanogap resonance overlaps with the excitation and detection wavelengths.[31] In our experiments, this optimal gap size is at around 10 nm for an excitation wavelength of 633 nm. Interestingly, this optimal gap size shifts to 5 nm, when the same pattern is excited at 785 nm, as shown in Figure 1f and in good agreement with the calculated red-shift of the gap plasmon resonance for smaller gap sizes. Additionally, we observe a quenching of the resonance for gap sizes below 5 nm, when Au crystallites on opposing sidewalls start to intersect. Nanogap resonators are therefore prone to resonance matching since varying only the gap size controls the resonance wavelength. In contrast, the resonance of dipole antennas with nanometric gaps is mostly affected by the antenna size, but also by the gap size, which leads under resonance matching conditions to highest near-field enhancement where the antenna patterns are operated at the smallest gap.[15]

Let us now study the influence of the gap sidewall length on SERS by varying the Au layer thickness between 30 and 100 nm, Figure 2a and b, for a given nanogap size. Remarkably, with 10 nm gap arrays strong SERS signals appear only when the Au layer thickness is above 60 nm, Figure 2e. After a steep rise, the SERS intensity levels off around a thickness of 100 nm, suggesting that a minimum cavity length is required to allow for Fabry–Perot type gap plasmons. Indeed, we obtain by calculation that, for a 10 nm gap with 100 nm long sidewalls, the fundamental, lowest order Fabry–Perot mode is an antisymmetric MIM plasmon, Figure 2d. The fundamental mode of such a gap plasmon corresponds to a dipolar charge distribution at each metal sidewall with one node corresponding to a phase change of π.[24,32] The longitudinal modal size of the fundamental MIM gap plasmon mode has been shown to range between 80 and 110 nm,[22,32,33] in good agreement with the metal layer thickness onset for which we measure strong SERS enhancement. Below 80 nm metal thickness, gap plasmon modes cannot exist, and thus the observed near-field intensity in the gap region, Figure 2c, and the SERS signal are minimal.

During the angular evaporation, metal is also deposited onto the sidewall of the photoresist, producing the sharp metal apex visible in Figure 2b. For thin metal layers, this apex forms a crescent-like nano structure. Its resonance is found to be extremely sensitive to sub-Ångström changes of the gap opening and thus is a measure of the plasmon radiance.[34] For our case, the metal tapering enables an efficient coupling of the external field to the plasmon mode. It has been previously shown that gap plasmon modes can lead to highly localized near-field hotspots, but to achieve strong SERS enhancement this plasmonic mode must also be efficiently coupled to the incident field[34] and scatter back into the far-field.[35] For nanogap resonator arrays, the top surface consists mostly of a flat metal film with high reflectivity and therefore a low coupling efficiency. By tapering the opening of the nanogap region, the coupling of the incident field to the gap plasmon mode is enhanced and the incoming energy guided to the nanogap mode by adiabatic compression.[36−39] To explore this

dx.doi.org/10.1021/nl403030g | Nano Lett. 2013, 13, 5449−5453

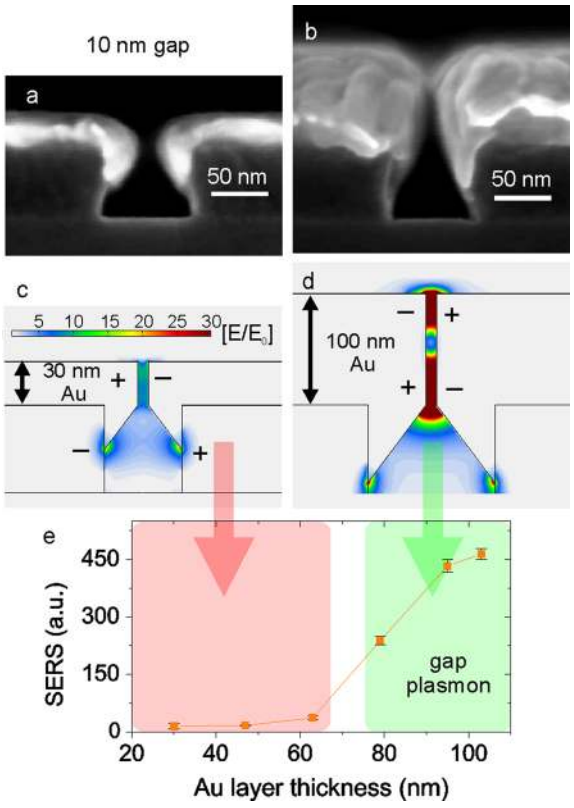

Figure 2. Gap plasmon modes at varying metal layer thickness. (a and b) Cross section SEM images; (c and d) simulated near-field maps at a wavelength of 650 nm for two different Au thicknesses of 30 and 100 nm. (e) SERS enhancement of a 10 nm gap arrays with varying Au metal thicknesses. The intensities correspond to the 1008 cm^{-1} Raman shift peak of a self-assembled benzene-ethane-thiol monolayer. Error bars represent the standard deviation of 16 spatially separated SERS measurements.

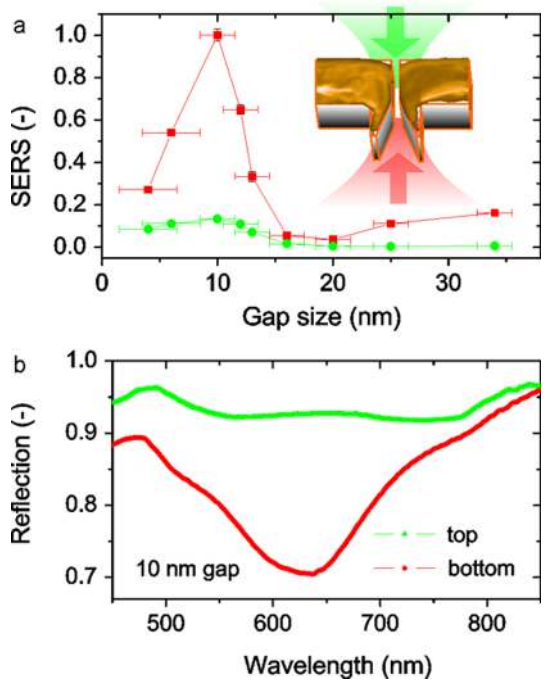

Figure 3. Influence of the excitation side of a 100 nm thick gap array on a glass substrate with excitation either from the top (green) or the bottom (red). (a) The SERS intensity of the 1008 cm^{-1} peak of a self-assembled benzene-ethane-thiol monolayer with varying gap sizes and (b) the pattern reflection of a 10 nm gap array. Error bars represent the standard deviation of 16 spatially separated SERS measurements and the analysis of multiple SEM images. The excitation, polarization, and integration times were kept constant for all measurements.

coupling effect, we compare in Figure 3 the SERS enhancement and visible to near-infrared reflection for a 100 nm thick pattern with 10 nm gaps that are excited either from the flat top or the tapered bottom side. We observe a 7-fold increase in the SERS intensity for excitation from the bottom side, compared to the top side, in Figure 3a. This increase of SERS enhancement is assigned to an improved coupling efficiency. The latter we estimate from the plasmonic radiance[34] obtained from the comparison of the top and bottom reflection as compared to a continuous Au film from an unpatterned area, Figure 3b. While we observe for the 10 nm gap structure a broadband absorption with 6% magnitude for top side excitation, a distinct resonance dip in reflection with 30% magnitude is observed when the pattern is excited from the bottom side. We cannot discuss the resonance position due to the broadband effect under top side excitation, but from the resonance magnitude we estimate a 5-fold increase in the coupling efficiency- This could ideally lead to a 25× increase in SERS intensity, while we only observe a gain of 7×. In comparison with the far-field simulations from Figure 1 the observed resonances are much broader and smaller in magnitude. We attribute this to gap size dispersions and roughness of the investigated structure. In agreement with the coupling model, the SERS intensity dependence on the gap size of the 100 nm thick pattern follows the same trend for either excitation side, with an optimum gap at about 10 nm. Hence, the same gap plasmon mode is excited from both sides, although more efficiently from the bottom side.

In the following, we compare the top with bottom side excitation scheme to a nanopattern enclosed in a liquid cell filled with ethanol. In this case, not only is the SERS intensity from the analyte monolayer for bottom side excitation improved by a factor of 10 compared to top side excitation, but also the background signal from the ethanol is suppressed by a factor of 2, as shown in Figure S3 of the Supporting Information. Taking into account that the optical path for bottom side excitation does not cross the analyte solution flowing on the top side of the structure, we can conclude that the SERS background is dominantly generated by molecules near or in the nanogap opening.

So far, we have discussed the enhancement factor of a slit array with 250 nm periodicity averaged over the excitation spot which is expected to be about 1.5 μm from $1.22\lambda_{laser}$/NA. The thus-obtained SERS intensities show a standard deviation below 4% across a patterned area of 0.5 mm^2 with a histogram given in Figure S2 of the Supporting Information. We calculate a surface averaged SERS enhancement factor of 10^6 for a 10 nm gap array under backside excitation, assuming that all molecules on the surface and in the focal spot contribute to the signal (details in the Supporting Information). This conservative enhancement factor is similar to values reported for nanogap resonators, although the local enhancement factor can be assumed larger,[11] whereby we do not know the exact number of molecules contributing to SERS. To investigate the SERS signal dependence associated with the number of illuminated slits, nanogap resonators are prepared with gap periodicities between

dx.doi.org/10.1021/nl403030g | Nano Lett. 2013, 13, 5449−5453

15 μm and 250 nm using electron-beam lithography. By scanning the laser excitation spot across the gap, we can resolve the Raman signal from individual nanogaps, once the slits are well-separated; see inset in Figure 4. The average SERS signal is

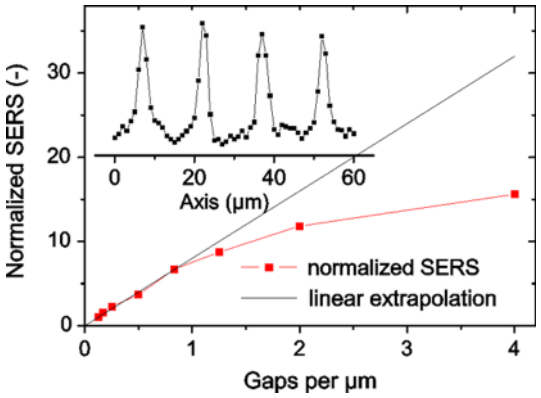

Figure 4. SERS intensity related to varying the nanogap periodicity. The gap arrays were fabricated with electron-beam lithography and angular evaporation. The SERS signal corresponds to the 1008 cm^{-1} Raman shift of a self-assembled benzene-ethane-thiol monolayer and was normalized to the intensity at a period of 8 μm. The periodicity is expressed as the number of gaps per micrometers. For the average SERS signal, the focal spot was continuously deflected within a field of 20 × 20 μm during the SERS signal integration of 5 s. The inlet shows a SERS scan across four nanogaps with a period of 15 μm, recorded without the laser focal spot deflection.

taken by integrating the Raman signal while scanning the laser beam over an area of 20 × 20 μm^2. We obtain a linear increase of the SERS intensity when plotted against the gap density up to a gap packing of almost 1 gap per μm that originates from the linear increase of molecules contributing to the SERS signal. Above 1 gap per μm, the average SERS intensity deviates from the linear trend and saturates for densities higher than about 2 μm^{-1}, as seen in Figure 4. For high gap densities, the individual gap plasmon modes might interfere which decreases the optimal coupling efficiency of each individual gap plasmon. We assume that the SERS saturation results from inefficient coupling to the gap plasmon modes leading to a reduced near field intensity. From this we can immediately conclude that such nanogap arrays do not need to be denser than 1−2 slits per μm, which makes it possible to produce such structures by cheaper mass fabrication methods.[28] Disregarding the detailed mechanism leading to the funneling of light into the nanogaps, we like to mention that in extraordinary optical transmission (EOT) efficient funneling is observed up to the propagation length of surface plasmons of roughly 3 μm for Au at a wavelength of 633 nm.[40−42] Interestingly, the width of the SERS signal recorded when scanning normal to the vertical direction of the slit is considerably larger (± factor of 2) than the expected 1.5 μm, Figure 4; this could either be related to the above-mentioned collection mechanism or to the recently introduced magnetoelectric interference effect.[43] The latter model predicts that the energy flow, that is, the funneling of light, is described as the interference between evanescent and propagating fields. This effect thus predicts collection diameters related to the amplitude decay length of involved fields, which is larger than the intensity decay length typically by $2^{1/2}$.

In summary, nanogap resonator arrays enable strong near-field enhancement for SERS measurements and can be fabricated over large arrays with a scalable technique based on interference lithography and angular evaporation, enabling accurate gap sizes below 10 nm. Such arrays represent an inexpensive alternative to nanoparticle based gap arrays requiring high-resolution lithography. Resonance matching with the excitation wavelength is shown to be crucial, as the resonance strongly depends on the gap size, the optimum gap being not necessarily the smallest one. Most importantly, gap plasmon modes require a minimal cavity length defined by the metal layer thickness (about 80 nm in our experiments) in order to allow for a standing wave Fabry−Perot mode. Another limitation comes from the coupling requirement to gap plasmon modes, as flat nanogap arrays can be highly reflective. We have measured a 10× increase of the SERS intensity by tapering the backside of the array with a conical gap opening obtained as a byproduct of the angular evaporation. Additionally, suppression of solvent background signals is achieved under backside excitation. Finally, we observed saturation of the SERS intensity for nanogap periods below 1 μm because the incident field is distributed to multiple gap modes. We pinpoint the trade-off between highest average SERS enhancement and the demand for higher resolution lithography, at a period of about 500 nm, which is well achievable by low-cost lithography.[28]

To conclude, nanogap resonator arrays offer substantial advantages for sensitive and reproducible sensing experiments and can be fabricated without high-resolution and cost-intensive lithography steps over wafer scale dimensions. The presented angular evaporation scheme is broadly applicable and leads to a self-limiting sub-10 nm gap precision used for maximum near-field enhancement. Combined with a fiber-based SERS probe, molecules could be analyzed remotely, while background signals from surrounding molecules in solution are suppressed. Together with a sensor cleaning method, such a sensor probe can be made reusable without losing the signal enhancement factor.[44]

■ ASSOCIATED CONTENT

Ⓢ Supporting Information

Schematic and fabrication details leading to sub-10 nm gap arrays, experimental methods, and simulation details; SERS histogram of a 12 nm gap array and details of the enhancement factor calculation; SERS spectra recorded in a liquid cell under top and bottom excitation. This material is available free of charge via the Internet at http://pubs.acs.org.

■ AUTHOR INFORMATION

Corresponding Author

*E-mail: thomas.siegfried@psi.ch.

Notes

The authors declare no competing financial interest.

■ ACKNOWLEDGMENTS

T.S. would like to thank R. Ernst, for using his private Raman setup for measurements at 785 nm and the introduction to Tibetan art. This work was supported by the Swiss National Science Foundation (SNF). Part of this work was performed at the Swiss Light Source (SLS), Paul Scherrer Institute, Switzerland.

■ REFERENCES

(1) Kneipp, K.; Wang, Y.; Kneipp, H.; Perelman, L. T.; Itzkan, I.; Dasari, R. R.; Feld, M. S. *Phys. Rev. Lett.* **1997**, *78* (9), 1667−1670.

(2) Bantz, K. C.; Meyer, A. F.; Wittenberg, N. J.; Im, H.; Kurtulus, O.; Lee, S. H.; Lindquist, N. C.; Oh, S.-H.; Haynes, C. L. *Phys. Chem. Chem. Phys.* **2011**, *13* (24), 11551−11567.
(3) Halas, N. J.; Lal, S.; Chang, W.-S.; Link, S.; Nordlander, P. *Chem. Rev.* **2011**, *111* (6), 3913−3961.
(4) Ye, J.; Wen, F.; Sobhani, H.; Lassiter, J. B.; Dorpe, P. V.; Nordlander, P.; Halas, N. J. *Nano Lett.* **2012**, *12* (3), 1660−1667.
(5) Novotny, L.; Hecht, B. *Principles of Nano-Optics*; Cambridge University Press: New York, 2012.
(6) Lindquist, N. C.; Nagpal, P.; McPeak, K. M.; Norris, D. J.; Oh, S.-H. *Rep. Prog. Phys.* **2012**, *75* (3), 036501.
(7) Bora, M.; Fasenfest, B. J.; Behymer, E. M.; Chang, A. S. P.; Nguyen, H. T.; Britten, J. A.; Larson, C. C.; Chan, J. W.; Miles, R. R.; Bond, T. C. *Nano Lett.* **2010**, *10* (8), 2832−2837.
(8) Ciraci, C.; Hill, R. T.; Mock, J. J.; Urzhumov, Y.; Fernandez-Dominguez, A. I.; Maier, S. A.; Pendry, J. B.; Chilkoti, A.; Smith, D. R. *Science* **2012**, *337* (6098), 1072−1074.
(9) Duan, H.; Hu, H.; Kumar, K.; Shen, Z.; Yang, J. K. W. *ACS Nano* **2011**, *5* (9), 7593−7600.
(10) Hatab, N. A.; Hsueh, C.-H.; Gaddis, A. L.; Retterer, S. T.; Li, J.-H.; Eres, G.; Zhang, Z.; Gu, B. *Nano Lett.* **2010**, *10* (12), 4952−4955.
(11) Im, H.; Bantz, K. C.; Lindquist, N. C.; Haynes, C. L.; Oh, S.-H. *Nano Lett.* **2010**, *10* (6), 2231−2236.
(12) Stosch, R.; Yaghobian, F.; Weimann, T.; Brown, R. J. C.; Milton, M. J. T.; Güttler, B. *Nanotechnology* **2011**, *22* (10), 105303.
(13) Theiss, J.; Pavaskar, P.; Echternach, P. M.; Muller, R. E.; Cronin, S. B. *Nano Lett.* **2010**, *10* (8), 2749−2754.
(14) Ward, D. R.; Huser, F.; Pauly, F.; Cuevas, J. C.; Natelson, D. *Nat. Nanotechnol.* **2010**, *5* (10), 732−736.
(15) Duan, H.; Fernández-Domínguez, A. I.; Bosman, M.; Maier, S. A.; Yang, J. K. W. *Nano Lett.* **2012**, *12* (3), 1683−1689.
(16) Zuloaga, J.; Prodan, E.; Nordlander, P. *Nano Lett.* **2009**, *9* (2), 887−891.
(17) Haynes, C. L.; Van Duyne, R. P. *J. Phys. Chem. B* **2001**, *105* (24), 5599−5611.
(18) Wen, X.; Xi, Z.; Jiao, X.; Yu, W.; Xue, G.; Zhang, D.; Lu, Y.; Wang, P.; Blair, S.; Ming, H. *Plasmonics* **2013**, *8* (2), 225−231.
(19) Wang, H.; Levin, C. S.; Halas, N. J. *J. Am. Chem. Soc.* **2005**, *127* (43), 14992−14993.
(20) Im, H.; Bantz, K. C.; Lee, S. H.; Johnson, T. W.; Haynes, C. L.; Oh, S.-H. *Adv. Mater.* **2013**, *25* (19), 2678−2685.
(21) Siegfried, T.; Ekinci, Y.; Solak, H. H.; Martin, O. J. F.; Sigg, H. *Appl. Phys. Lett.* **2011**, *99* (26), 263302.
(22) Søndergaard, T.; Siahpoush, V.; Jung, J. *Phys. Rev. B* **2012**, *86* (8), 085455.
(23) Belotelov, V. I.; Kalish, A. N.; Zvezdin, A. K.; Gopal, A. V.; Vengurlekar, A. S. *J. Opt. Soc. Am. B* **2012**, *29* (3), 294−299.
(24) Kern, J.; Großmann, S.; Tarakina, N. V.; Häckel, T.; Emmerling, M.; Kamp, M.; Huang, J.-S.; Biagioni, P.; Prangsma, J. C.; Hecht, B. *Nano Lett.* **2012**, *12* (11), 5504−5509.
(25) Auzelyte, V.; Dais, C.; Farquet, P.; Grutzmacher, D.; Heyderman, L. J.; Luo, F.; Olliges, S.; Padeste, C.; Sahoo, P. K.; Thomson, T.; Turchanin, A.; David, C.; Solak, H. H. *J. Micro/Nanolithogr., MEMS MOEMS* **2009**, *8* (2), 021204−10.
(26) Päivänranta, B.; Langner, A.; Kirk, E.; David, C.; Ekinci, Y. *Nanotechnology* **2011**, *22* (37), 375302.
(27) Abelmann, L.; Lodder, C. *Thin Solid Films* **1997**, *305* (1−2), 1−21.
(28) Fucetola, C. P. *J. Vac. Sci. Technol., B* **2009**, *27* (6), 2958.
(29) Siegfried, T.; Ekinci, Y.; Martin, O. J. F.; Sigg, H. *ACS Nano* **2013**, *7* (3), 2751−2757.
(30) Gallinet, B.; Kern, A. M.; Martin, O. J. F. *J. Opt. Soc. Am. A* **2010**, *27* (10), 2261−2271.
(31) Kern, A. M.; Meixner, A. J.; Martin, O. J. F. *ACS Nano* **2012**, *6* (11), 9828−9836.
(32) Søndergaard, T.; Jung, J.; Bozhevolnyi, S. I.; Valle, G. D. *New J. Phys.* **2008**, *10* (10), 105008.
(33) Jung, J.; Søndergaard, T.; Bozhevolnyi, S. I. *Phys. Rev. B* **2009**, *79* (3), 035401.
(34) Gallinet, B.; Siegfried, T.; Sigg, H.; Nordlander, P.; Martin, O. J. F. *Nano Lett.* **2012**, *13* (2), 497−503.
(35) Weihua, Z.; Fischer, H.; Schmid, T.; Zenobi, R.; Martin, O. J. F. *J. Phys. Chem. C* **2009**, *113* (33), 14672−14675.
(36) Choo, H.; Kim, M.-K.; Staffaroni, M.; Seok, T. J.; Bokor, J.; Cabrini, S.; Schuck, P. J.; Wu, M. C.; Yablonovitch, E. *Nat. Photonics* **2012**, *6* (12), 838−844.
(37) Ginzburg, P.; Arbel, D.; Orenstein, M. *Opt. Lett.* **2006**, *31* (22), 3288−3290.
(38) Lindquist, N. C.; Johnson, T. W.; Nagpal, P.; Norris, D. J.; Oh, S.-H. *Sci. Rep.* **2013**, *3*, 1857.
(39) Diwekar, M.; Davis, M.; Blair, S. *J. Nanophotonics* **2010**, *4* (1), 043504−043504-11.
(40) Bravo-Abad, J.; Degiron, A.; Przybilla, F.; Genet, C.; Garcia-Vidal, F. J.; Martin-Moreno, L.; Ebbesen, T. W. *Nat. Phys.* **2006**, *2* (2), 120−123.
(41) Fernández-Domínguez, A. I.; García-Vidal, F. J.; Martín-Moreno, L. *Phys. Rev. B* **2007**, *76* (23), 235430.
(42) Kolomenski, A.; Kolomenskii, A.; Noel, J.; Peng, S.; Schuessler, H. *Appl. Opt.* **2009**, *48* (30), 5683−5691.
(43) Pardo, F.; Bouchon, P.; Haidar, R.; Pelouard, J.-L. *Phys. Rev. Lett.* **2011**, *107* (9), 093902.
(44) Siegfried, T.; Kind, M.; Terfort, A.; Martin, O. J. F.; Zharnikov, M.; Ballav, N.; Sigg, H. *J. Raman Spectrosc.* **2012**, *44* (2), 170−175.